Multiple Quantum Well Retromodulators for Spacecraft-To-Spacecraft Laser Interrogation, Communication, and Navigation

N. Glenn Creamer, Ph.D.
Naval Research Laboratory, Code 8230, 4555 Overlook Avenue, Washington, DC 20375
gcreamer@space.nrl.navy.mil

G. Charmaine Gilbreath, Ph.D.
Naval Research Laboratory, Code 7215
gilbreath@rsd.nrl.navy.mil

Timothy J. Meehan
Naval Research Laboratory, Code 8121
meehan@ncst.nrl.navy.mil

Mena Ferraro Stell
Research Support Instruments
Lanham, MD 20706
ferraro@ncst.nrl.navy.mil

Michael J. Vilcheck
Naval Research Laboratory, Code 8123
vilcheck@ncst.nrl.navy.mil

William S. Rabinovich, Ph.D.
Naval Research Laboratory, Code 5654
rabinovich@nrl.navy.mil

Abstract.

This paper describes a novel concept for laser-based interrogation, communication, and navigation between multiple spacecraft platforms using a gimbaled laser source on a pursuer spacecraft and a target board populated with retromodulators (modulating retroreflectors) integrated on a host spacecraft. The combined laser source and retroreflectors can provide centimeter-level relative positioning between each vehicle, as well as spacecraft-to-spacecraft laser communication via semiconductor-based Multiple Quantum Well retromodulators. Additionally, strategies are developed for utilizing the target board retromodulator array to provide relative attitude between each vehicle. In this scenario, each reflector has its own unique modulating code sequence, allowing the returned signals to be discriminated and processed by the pursuer spacecraft to determine the relative orientation. Based on additional attitude sensing capability, three classes of host spacecraft are considered: fully-cooperative, partially-cooperative, and non-cooperative. Numerical simulations using a five-sensor target board demonstrate the potential of the concept, and preliminary test results demonstrate reflector discrimination capability.

Introduction

Due to the many obvious benefits of autonomous spacecraft-to-spacecraft interrogation, communication, and relative navigation for civilian, commercial, and military space missions, there has been a significant amount of research and development on associated relative sensor systems over the past few years.[1-9] These systems typically implement radio-frequency communication links to utilize GPS sensing for long-range relative positioning and combinations of visual and laser ranging for short-range proximity operations.

The relative GPS system places the estimated target location inside the error sphere of the visual sensor at about a 100-meter range for easy sensor handoff. The visual/laser system is then utilized for all subsequent short-range operations such as formation flying, inspection, and docking. Of course, this approach requires the host (or target) spacecraft to possess an RF antenna and transmitter along with a GPS sensor to transmit its navigational data to the pursuer spacecraft. Additionally, this concept is not suitable for geosynchronous or deep space missions due to lack of GPS signal, unless a GPS-type system is emulated

1

between each vehicle.[2] Although the visual/laser systems provide sufficiently accurate relative state estimation for close-in operations (i.e. 0 to 30 meters), their mid- to long-range capability (i.e. >50 meters) is significantly cruder, with relative position and attitude errors reaching 10 meters and 10 degrees at ranges exceeding 80-100 meters.

In this paper we develop a novel concept utilizing solid-state multiple quantum well (MQW) retromodulators to provide spacecraft-to-spacecraft laser communication and navigation (relative position and orientation). The device enables compact, low power, and low mass optical data transfer.[10] Data transfer can be on the order of megabits per second, depending on link characteristics, with relative navigation on the order of centimeters in position and a few degrees in orientation. Links over ranges of kilometers down to tens of meters are possible. For proximity operations of about 30 meters or less (docking missions, for example) this concept can work harmoniously with a vision-based system to provide relative communication and navigation with minimal sacrifice in host power and weight.

MQW Retromodulators

Device Description

Modulating retroreflector (MRR) systems using MQW technology provide a low power, low weight, multi-functional solution to the need to reduce parasitic payload requirements from conventional communications technologies. A modulating retroreflector is a solid-state device that allows optical communication and ranging between two platforms. MQW shutters are particularly suited to these applications because the technology enables fast data rates, requires very low drive powers, is lightweight, robust, and is not polarization-sensitive.[11,12] (See the Naval Research Laboratory MRR web page at http://mrr.nrl.navy.mil.)

Implementation of such a device requires that only one of the platforms have an onboard laser, telescope, and tracker. Thus, the device is well suited to problems in which one platform has a large payload capacity and can serve as the interrogator and the other platform does not. The interrogator illuminates the platform carrying the modulating retroreflector with a laser beam. The laser beam is automatically reflected back with no need for pointing or tracking. The reflected return is modulated in an On Off Keying (OOK) mode.

Bi-directional communications can occur if a lower data rate is imposed on the interrogation beam. The modulated retroreflected signal is then received in a burst communications mode. Detectors on the retroreflector platform can receive the transmitted signal, which may inform the smaller platform of interrogator ID, or location details, etc. These detectors can also receive photonic information which can be used in acquisition and tracking. A representative concept is illustrated in Figure 1.

The modulator must have several characteristics to make a link possible. The shutter must have a high switching speed, low power consumption, large area, wide field-of-view, and high optical quality. In addition, it must work at wavelengths where good laser sources are available, be radiation-tolerant (for space applications) and rugged. Semiconductor multiple quantum well modulators are one of the few technologies that meet all these requirements.[13,14]

These devices are based upon the same materials technology as laser diodes. They consist of several hundred very thin (~10 nm) layers of semiconductor material, such as GaAs, deposited on a large (7.6 cm diameter) semiconductor wafer. Electrically, they take the form of a P-I-N diode. Optically, the thin layers induce a sharp absorption feature at a wavelength that is determined by the constituent materials and the structure that is grown. When the device has a moderate (~15V) voltage placed across it in reverse bias, the absorption feature changes, both shifting to longer wavelengths and dropping in magnitude. Thus, the transmission of the device near this absorption feature changes dramatically and can serve as an on-off shutter. This switching capability is shown in Figure 2 for an InGaAs-based MQW modulator that was designed and grown for use in an optical link. The device is grown on an n-type GaAs wafer and is capped by a p-type contact layer, thus forming a P-I-N diode. It is a transmissive modulator designed to work at a wavelength of 980 nm, compatible with many good laser diode sources.

Unlike liquid crystal modulators, MQW modulators have very high switching speeds. Small devices (diameters of microns) have been operated at speeds in the tens of GHz. In practice, the speed is limited primarily by the RC time of the device. Thus, the large area devices (on the order of a centimeter) used for retromodulator-based communications typically have speeds between 1 and 10 Mbps. Higher speeds are possible, however, depending on range and the sophistication of the fabrication process. In practice, data rates like these are appropriate for many of the sensors carried on the small platforms for which these devices are intended.

2

Glenn Creamer

15th Annual AIAA/USU Conference on Small Satellites

Data Link Considerations

In practice, except for close ranges, the link rather than the modulator limits performance of a modulating retro system. For a conventional corner-cube modulating retroreflector, MQW technology should allow data rates in the tens of megabits per second, depending on the range and the interrogator system.

For a diffraction-limited system the optical power, retro-reflected from the small platform back to the large platform, scales as

$$\frac{P_{laser} \cdot D_{retro}{}^4 \cdot D_{rec}{}^2 \cdot T_{atm}{}^2}{\theta_{div}{}^2 \cdot \rho^4} \qquad (1)$$

where P_{laser} is the power of the laser transmitter on the large platform, D_{retro} is the diameter of the modulating retroreflector on the small platform, D_{rec} is the diameter of the receive telescope on the large platform, T_{atm} is the loss due to transmission through the atmosphere, θ_{div} is its divergence of the transmit beam, and ρ is the range between the two platforms.

The strongest dependencies are on the range and the retroreflector diameter, both of which scale as fourth powers. Retroreflector links fall off more strongly with range than conventional links because of their bi-directional nature. The strong dependence on retroreflector diameter occurs because increasing the size of the retroreflector both increases the optical power intercepted and decreases the divergence of the returned optical beam. The link is very clearly a compromise between a large retroreflector aperture to maximize the returned optical power and a small modulator to maintain data rate while keeping the consumed electrical power low. This trade is mitigated to some extent by using segmented devices discussed in the references. When all the segments are driven in parallel, the power consumption may be comparable to a monolithic device, but the modulation rate of the smaller device will be exploited while enabling the larger aperture. When the drive voltage waveform is optimized, the electrical power consumption of a MQW modulating retroreflector scales as

$$D_{mod}{}^4 \cdot V^2 B^2 R_S \qquad (2)$$

where D_{mod} is the diameter of the modulator, V is the voltage applied to the modulator (fixed by the required optical contrast ratio), B is the maximum data rate of the device, and R_S is the sheet resistance of the device.

An example of a waveform recorded using a 9-segmented device illustrating 10 megabits per second is shown in Figure 3.

Time-Of-Flight Range Capability

Range measurements to each MRR within an array are determined from time-of-flight (TOF) techniques, similar to the approach used by laser range finders for surveying. The unique aspect of our concept is the ability to selectively range each MRR with one all-illuminating laser beam. This is accomplished through the modulation logic. The TOF is determined by measuring the round-trip time it takes a pulse to travel from the laser diode to the reflector and back. From the speed of light, c, the range becomes

$$\rho = \tfrac{1}{2}\,(\text{TOF} * c) \qquad (3)$$

Clearly, range errors are linearly related to random noise and bias errors in the TOF measurements. Through multi-shot averaging, random noise errors can be attenuated by the square-root of the number of samples. The bias errors are due to un-calibrated stray returns from MRRs that are set in the low or "off" state.

Reflector Code Sequence Discrimination

Reflector discrimination is achieved through a set of matching filters tuned to each MRR's unique modulator code sequence, as depicted in Figure 4. The return photons are collected on the photodetector and converted to digital signals via an analog-to-digital converter. The digital signals are then processed through each of the uniquely tuned matching filters to isolate the return signals from each MRR. These signals are then used to determine the ranges to each MRR and decode any return data streams.

Relative Pose Estimation using MRR Arrays

The reflected signals from a distributed array of MRRs can provide both relative position and attitude information. Although a variety of array geometries can be utilized, we choose to study the diamond-and-one configuration depicted in the photograph of Figure 5, where four MRRs form the corners of a square diamond with side length L, and a fifth MRR is included as a centering source whose signal intensity is maximized during initial acquisition and track. As described in the previous section, each reflected signal is modulated at a unique code sequence to allow discrimination and signal isolation between each MRR in the array.

3

We define *relative pose P* of a host spacecraft with respect to a pursuer spacecraft as the combined state vector consisting of relative position states and relative attitude states. In the following we derive pose estimation logic for three classes of host spacecraft:

- A *Fully-Cooperative Host* that provides complete three-axis attitude knowledge to the pursuer. Examples may include one member of a formation-flying constellation, a manned space station, or an orbiting fluid storage platform.

- A *Partially-Cooperative Host* that provides a measured body-fixed unit vector of some reference entity (i.e. the local geomagnetic field, the Sun vector, or the Earth vector) to the pursuer. Examples may include a minimally-instrumented orbiting commodity bank or one end of a space tether.

- A *Non-Cooperative Host* that provides no attitude information to the pursuer. An example may be a non-instrumented, passively-stabilized orbiting commodity bank.

In each case we assume the pursuer spacecraft possesses complete attitude and orbit determination and control capability.

Fully-Cooperative Host

For this class of spacecraft the host has complete attitude determination capability relative to a known reference frame and incorporates this information on the modulated optical signal returned to the pursuer. In this case the MRR array of Figure 5 is redundant and we actually need only one modulated reflector to provide the necessary information. Upon receiving the modulated signal, the pursuer spacecraft calculates the range to the MRR from equation (3) and the relative position vector from the laser gimbal angles and calculated range using the relation

$$\mathbf{R}^{P} = \rho \hat{\boldsymbol{l}}^{P} \qquad (4)$$

where ρ is the calculated relative range, $\mathbf{R}^{P}$ is the relative position vector expressed in the pursuer frame, and $\hat{\boldsymbol{l}}^{P}$ is the associated relative unit vector expressed in the pursuer frame. This unit vector is determined from the laser gimbal azimuth and elevation angles. The relative attitude is obtained from the direction cosine matrix (DCM) transformation

$$\mathbf{C}_{H/P} = \mathbf{C}_{H/R}\mathbf{C}_{P/R}^{T} \qquad (5)$$

where $\mathbf{C}_{H/P}$ is the DCM of the host frame relative to the pursuer frame, $\mathbf{C}_{H/R}$ is the DCM of the host frame relative to the reference frame, $\mathbf{C}_{P/R}$ is the DCM of the pursuer frame relative to the reference frame, and T represents the matrix transpose function. Utilizing this complete relative pose information and its own control system, the pursuer spacecraft can position and orient itself relative to the host as required by mission operations.

Partially-Cooperative Host

For this class of spacecraft the host possesses one sensor capable of measuring a body-fixed unit *entity* vector $\hat{\mathbf{e}}^{H}$ in the host frame of, for example, the local geomagnetic field (from a magnetometer), the local Sun direction (from a Sun sensor), or the local Earth direction (from an Earth sensor). Depending on the processing capability of the host spacecraft, either the processed entity vector or the raw sensor output can be incorporated on the center MRR modulated return signal. Knowing the position of the pursuer spacecraft relative to the reference frame from its orbit determination capability and the position of the host spacecraft relative to the pursuer spacecraft from equation (4), we can determine the unit entity vector measurement expressed in the pursuer frame *at the host location* from the relation

$$\hat{\mathbf{e}}^{P} = \mathbf{C}_{P/R}\hat{\mathbf{e}}^{R} \qquad (6)$$

where $\hat{\mathbf{e}}^{R}$ is obtained from the position of the host spacecraft in the reference frame and the known position/orientation of the reference vector being measured (i.e. the geomagnetic field), and $\mathbf{C}_{P/R}$ is known from the pursuer attitude determination system.

Knowledge of the measured entity vector $\hat{\mathbf{e}}$ in both the pursuer and host frames is insufficient to determine the complete relative attitude of the host (two non-colinear vectors must be known in each frame to uniquely determine the relative attitude). Therefore, we utilize the range information from the remaining MRRs in the array to provide an additional vector measurement. Referring to Figure 5, we choose the two host-fixed vectors $\mathbf{r}_{AC}^{H}$ and $\mathbf{r}_{BD}^{H}$ to maximize baseline length. Using the geometry of Figure 6 and the law of cosines,

4

it can be shown that the ranges to the MRRs defining the host unit basis vectors satisfy the relations

$$\cos\theta_1 = \frac{\rho_C^2 - \rho_A^2}{2\left|\mathbf{r}_{AC}^H\right|\rho_E} \tag{7a}$$

$$\cos\theta_2 = \frac{\rho_D^2 - \rho_B^2}{2\left|\mathbf{r}_{BD}^H\right|\rho_E} \tag{7b}$$

where the ranges are determined from the modulated return signals of each MRR, θ_1 is the angle between $\hat{l}^P$ and the host $\hat{\mathbf{h}}_1$ unit basis vector, and θ_2 is the angle between $\hat{l}^P$ and the host $\hat{\mathbf{h}}_2$ unit basis vector. It is clear that the effect of errors in the measured ranges (i.e. random noise) will be attenuated by the inverse of the baseline lengths; hence, accuracy is proportional to the length of the baselines defined in the MRR array. After solving for the direction cosines, the unit vector $\hat{l}$ can be expressed in the host frame components as

$$\hat{l}^H = \cos\theta_1\,\hat{\mathbf{h}}_1 + \cos\theta_2\,\hat{\mathbf{h}}_2 \\ - \sqrt{1 - \cos^2\theta_1 - \cos^2\theta_2}\,\hat{\mathbf{h}}_3 \tag{8}$$

We now have two unit vector measurements represented in both the pursuer and host frames ($\hat{l}^P, \hat{l}^H, \hat{\mathbf{e}}^P, \hat{\mathbf{e}}^H$), and can uniquely determine the relative quaternion (and DCM, if desired) using the Quaternion Estimator (QUEST) method.[15] For this specific application the QUEST algorithm provides an estimate of the relative quaternion by optimizing the weighted loss function

$$J = \tfrac{1}{2}\left\{ w_1\left|\hat{l}^H - \mathbf{C}_{H/P}\hat{l}^P\right|^2 + w_2\left|\hat{\mathbf{e}}^H - \mathbf{C}_{H/P}\hat{\mathbf{e}}^P\right|^2 \right\} \tag{9}$$

where w_1 and w_2 are the measurement weighting parameters associated with the laser vector and the entity vector, respectively. The weights are typically chosen to be the inverse of the measurement variances. It can be shown[15] that the optimal quaternion $\mathbf{q}_{opt}$ satisfies the eigenvalue problem

$$\mathbf{K}\mathbf{q}_{opt} = \lambda_{max}\mathbf{q}_{opt} \tag{10a}$$

$$\mathbf{K} = \begin{bmatrix} \mathbf{S} - \sigma\mathbf{I}_3 & \mathbf{Z} \\ \mathbf{Z}^T & \sigma \end{bmatrix} \tag{10b}$$

$$\lambda_{max} = \sqrt{w_1^2 + w_2^2 + 2w_1 w_2 U_{12}} \tag{10c}$$

$$U_{12} = (\hat{l}^H \cdot \hat{\mathbf{e}}^H)(\hat{l}^P \cdot \hat{\mathbf{e}}^P) \\ + \left|\hat{l}^H \times \hat{\mathbf{e}}^H\right|\left|\hat{l}^P \times \hat{\mathbf{e}}^P\right| \tag{10d}$$

$$\mathbf{S} = w_1\left\{\hat{l}^H(\hat{l}^P)^T + \hat{l}^P(\hat{l}^H)^T\right\} \\ + w_2\left\{\hat{\mathbf{e}}^H(\hat{\mathbf{e}}^P)^T + \hat{\mathbf{e}}^P(\hat{\mathbf{e}}^H)^T\right\} \tag{10e}$$

$$\mathbf{Z} = w_1\hat{l}^H \times \hat{l}^P + w_2\hat{\mathbf{e}}^H \times \hat{\mathbf{e}}^P \tag{10f}$$

$$\sigma = w_1\hat{l}^H \cdot \hat{l}^P + w_2\hat{\mathbf{e}}^H \cdot \hat{\mathbf{e}}^P \tag{10g}$$

where $\mathbf{I}_3$ represents the 3x3 identity matrix. Hence, upon solving for the maximum eigenvalue from equation (10c), the optimal quaternion can be determined from solution of equation (10a), subject to the normalization

$$\mathbf{q}^T\mathbf{q} = 1 \tag{11}$$

Solutions to the eigenvalue problem for the general case of *n* measurement vectors is also described in Reference 15.

Similar to the previous class of host spacecraft, the pursuer spacecraft can utilize this complete relative pose information and its own control capability to position and orient itself relative to the host as required by mission operations.

Non-Cooperative Host

For this class of spacecraft the host has no attitude determination capability and, hence, provides no additional information to the pursuer other than the reflected, frequency-discriminated signal returns from each MRR. Therefore, in addition to the relative position vector derived from the center MRR, the only other discernible information from the MRR array is the angle of the array plane relative to the directional unit vector $\hat{l}$. This angle can be determined from equations (7a) and (7b), yielding

Glenn Creamer

15th Annual AIAA/USU Conference on Small Satellites

$$\phi = \frac{\pi}{2} - \cos^{-1}(\sqrt{1 - \cos^2\theta_1 - \cos^2\theta_2}) \qquad (12)$$

where ϕ is the angle between the $\hat{\mathbf{h}}_1 - \hat{\mathbf{h}}_2$ plane and $\hat{l}$.

This limited amount of relative orientation may very well be sufficient for some formation-flying or inspection missions as well as for mid- to long-range phases of rendezvous and capture (prior to terminal-phase vision sensor handoff). However, under certain circumstances additional information about the orientation of the host can be postulated. For example, if it is known that the host is passively gravity-gradient stabilized then, to within a few degrees, it can be assumed that the Earth nadir direction is along the minor principal axis, providing an approximate unit entity vector $\hat{\mathbf{e}}$ expressed in the host and pursuer frames. As another practical example, if it is known that the host is passively magnetic stabilized then, to within a few degrees, it can be assumed that the host spacecraft magnet is aligned with the local geomagnetic field, once again providing an approximate unit entity vector in the host and pursuer frames. Given these postulated entity vectors, the complete relative attitude can be estimated using the approach described in the previous section for partially-cooperative hosts.

System Error Sources

We categorize the potential system error sources into three classes: sensor errors, modeling errors, and geometric errors. Sensor errors include combined random noise and biases in the time-of-flight measurements, entity vector measurements, and laser gimbal angle measurements. Modeling errors include host baseline knowledge errors and slowly-varying biases due to assumptions on the entity vector motion of non-cooperative hosts. Geometric errors include effects due to orientation of the laser unit vector $\hat{l}$ relative to the entity vector measurement $\hat{\mathbf{e}}$ (errors increase as the two vectors approach co-linearity) and range-sensitive angular errors from the gimbaled laser tracking system. These latter errors are attributed to the fact that the laser can only be centered on a return signal to within approximately one-fourth of the total beam divergence required to encompass all the MRRs, defined as the baseline length divided by the range. For example, given a baseline of 0.5 meters at a range of 30 meters, the required beam divergence is 17 mrad and the laser pointing error is 0.24 degrees. We've attempted to quantify these various errors in Table 1, with the understanding that the actual numbers are mission and sensor dependent.

Kinematic Filter Formulation

To improve the accuracy of the instantaneous relative attitude estimation algorithms given in the previous section, we develop a kinematics-based Kalman filter to attenuate sensor noise effects and propagate the state estimate between sensor updates. We assume that the master spacecraft has rate gyros to sense kinematic rotational changes due to thruster and/or reaction wheel torques.

A filter architecture similar to the Uncoupled Lefferts, Markley, Shuster (ULMS) algorithm[16] is developed here. We begin by defining the rate vector of the host relative to the pursuer, expressed in the host frame, as

$$\boldsymbol{\omega} = \boldsymbol{\omega}_H^H - \boldsymbol{\omega}_P^H = \boldsymbol{\omega}_H^H - \mathbf{C}_{H/P}\boldsymbol{\omega}_P^P \qquad (13)$$

where $\boldsymbol{\omega}_H^H$ is the inertial rate of the host expressed in the host frame, $\boldsymbol{\omega}_P^H$ is the inertial rate of the pursuer expressed in the host frame, and $\boldsymbol{\omega}_P^P$ is the inertial rate of the pursuer expressed in the pursuer frame (as measured by the rate gyros). An expression for the rate error vector relative to the true rate vector $\boldsymbol{\omega}$ can now be written as

$$\begin{aligned} \boldsymbol{\omega}_e &= \boldsymbol{\omega} - \widetilde{\boldsymbol{\omega}} \\ &= (\boldsymbol{\omega}_H^H - \mathbf{C}_{H/P}\boldsymbol{\omega}_P^P) - (\widetilde{\boldsymbol{\omega}}_H^H - \widetilde{\mathbf{C}}_{H/P}\boldsymbol{\omega}_P^P) \quad (14) \\ &= \Delta\boldsymbol{\omega}_H^H - \Delta\mathbf{C}_{H/P}\boldsymbol{\omega}_P^P \end{aligned}$$

where $\widetilde{\boldsymbol{\omega}}_H^H$ and $\widetilde{\mathbf{C}}_{H/P}$ are the current best estimates of the host inertial body rates and the relative DCM, respectively.

The four-state quaternion describing the relative attitude of the host to the pursuer can be written as

$$\mathbf{q} = \left\{ \overline{\mathbf{q}}^T \quad q_4 \right\}^T \qquad (15a)$$

$$\overline{\mathbf{q}} = \left\{ q_1 \quad q_2 \quad q_3 \right\}^T \qquad (15b)$$

where $\mathbf{q}$ is the 4x1 quaternion, $\overline{\mathbf{q}}$ is the 3x1 vector portion, and q_4 is the scalar portion. This quaternion satisfies the kinematic relation

$$\dot{\mathbf{q}} = \tfrac{1}{2}\mathbf{\Omega}(\mathbf{\omega})\,\mathbf{q} \qquad (16a)$$

$$\mathbf{\Omega}(\mathbf{\omega}) = \begin{bmatrix} 0 & \omega_3 & -\omega_2 & \omega_1 \\ -\omega_3 & 0 & \omega_1 & \omega_2 \\ \omega_2 & -\omega_1 & 0 & \omega_3 \\ -\omega_1 & -\omega_2 & -\omega_3 & 0 \end{bmatrix} \qquad (16b)$$

We can define an error quaternion $\mathbf{q}_e$ relative to the true quaternion $\mathbf{q}$ from

$$\mathbf{q} = \widetilde{\mathbf{q}} \otimes \mathbf{q}_e \qquad (17)$$

where $\widetilde{\mathbf{q}}$ is the current best estimate of $\mathbf{q}$ and $\otimes$ is the quaternion multiplication operator. Following the procedure in Reference 16, it can be shown that, to first order in the error terms, the kinematic relation for the error quaternion becomes

$$\dot{\mathbf{q}}_e \approx \tfrac{1}{2}(\Delta\mathbf{\omega}_H^H - \Delta\mathbf{C}_{H/P}\,\mathbf{\omega}_P^P) - \widetilde{\mathbf{\omega}}\times\overline{\mathbf{q}}_e \qquad (18)$$

which can be furthered simplified by assuming small rates for each spacecraft, resulting in

$$\dot{\mathbf{q}}_e \approx \tfrac{1}{2}(\Delta\mathbf{\omega}_H^H) \qquad (19)$$

By assuming the host body rates are constant, the approximate error quaternion kinematics can be augmented with host rate error kinematic equations of the form

$$\Delta\dot{\mathbf{\omega}}_H^H \approx \mathbf{0} \qquad (20)$$

The resulting Kalman filter propagation equations for the estimated quaternion and host rates take on the form

$$\dot{\widetilde{\mathbf{q}}} = \tfrac{1}{2}\mathbf{\Omega}(\widetilde{\mathbf{\omega}})\,\widetilde{\mathbf{q}} \qquad (21a)$$

$$\dot{\widetilde{\mathbf{\omega}}}_H^H = \mathbf{0} \qquad (21b)$$

$$\dot{\mathbf{P}} = \mathbf{F}\mathbf{P} + \mathbf{P}\mathbf{F}^{\mathrm{T}} + \mathbf{Q} \qquad (21c)$$

$$\mathbf{F} = \begin{bmatrix} \mathbf{0} & \tfrac{1}{2}\mathbf{I}_3 \\ \mathbf{0} & \mathbf{0} \end{bmatrix} \qquad (21d)$$

where $\mathbf{P}$ and $\mathbf{Q}$ represent the 6x6 state covariance and user-defined process noise covariance matrices, respectively.

An approximate expression for the measured quaternion can be written as

$$(\mathbf{q})_{\mathrm{meas}} \approx \mathbf{q} \otimes (\mathbf{n},1) \qquad (22)$$

where $(\mathbf{q})_{\mathrm{meas}}$ is obtained from the techniques in the previous section, and $\mathbf{n}$ represents a 3x1 noise vector modeled as a zero-mean Gaussian process. Combining equations (14) and (19) leads to the desired measurement model

$$(\mathbf{q}_e)_{\mathrm{meas}} = \widetilde{\mathbf{q}}^{-1} \otimes (\mathbf{q})_{\mathrm{meas}} \approx \mathbf{q}_e \otimes (\mathbf{n},1) \qquad (23a)$$

$$(\overline{\mathbf{q}}_e)_{\mathrm{meas}} \approx \overline{\mathbf{q}}_e + \mathbf{n} = \mathbf{H}\begin{Bmatrix} \overline{\mathbf{q}}_e \\ \Delta\mathbf{\omega}_H^H \end{Bmatrix} + \mathbf{n} \qquad (23b)$$

$$\mathbf{H} = \begin{bmatrix} \mathbf{I}_3 & \mathbf{0} \end{bmatrix} \qquad (23c)$$

where $(\overline{\mathbf{q}}_e)_{\mathrm{meas}}$ is the vector portion of the measured quaternion error obtained from equation (23a) and $\mathbf{H}$ is the 3x6 measurement distribution matrix. The Kalman filter measurement update equations can now be written as

$$\mathbf{K} = \mathbf{P}\mathbf{H}^{\mathrm{T}}(\mathbf{H}\mathbf{P}\mathbf{H}^{\mathrm{T}} + \mathbf{R})^{-1} \qquad (24a)$$

$$\mathbf{P}^{+} = \mathbf{P} - \mathbf{K}\mathbf{H}\mathbf{P} \qquad (24b)$$

$$\begin{Bmatrix} \overline{\mathbf{q}}_e^{+} \\ \Delta\mathbf{\omega}_H^{H+} \end{Bmatrix} = \mathbf{K}\,(\overline{\mathbf{q}}_e)_{\mathrm{meas}} \qquad (24c)$$

$$\widetilde{\mathbf{q}}^{+} = \widetilde{\mathbf{q}} \otimes (\overline{\mathbf{q}}_e^{+}, 1) \qquad (24d)$$

$$\widetilde{\mathbf{\omega}}_H^{H+} = \widetilde{\mathbf{\omega}}_H^H + \Delta\mathbf{\omega}_H^{H+} \qquad (24e)$$

where $\mathbf{K}$ is the 6x3 Kalman gain matrix and $\mathbf{R}$ is the 3x3 measurement noise covariance matrix. Upon close inspection, it is clear from equations (21) through (24) that proper ordering of the six states $(\overline{\mathbf{q}}_e, \Delta\mathbf{\omega}_H^H)$ uncouples the filter about each axis as long as $\mathbf{Q}$ and $\mathbf{R}$ are diagonal, resulting in three simple two-state filters (one per axis). Additionally, further

7

Glenn Creamer

simplification can be achieved by implementing a steady-state or hybrid version of the two-state filters.[16]

Numerical Simulation

Relative navigation of a two-spacecraft leading/trailing formation is simulated in this section. The lead spacecraft serves as the host, containing a target board similar to the one in Figure 5 with one-meter baselines. The trailing spacecraft serves as the pursuer, whose objective is to determine the relative position and attitude of the host using a gimbaled laser tracker. The spacecraft are placed in the same orbit plane with an altitude of 600 km and an inclination of 60 degrees. The host spacecraft is stationed 100 meters ahead of the pursuer spacecraft, and both vehicles are aligned with the local-vertical, local-horizontal orbiting reference frame.

For this example we assume the host spacecraft possesses either an Earth sensor to measure the local nadir direction or a magnetometer to measure the local geomagnetic field. The Earth sensor has a 1-sigma noise error of 0.1 degrees and the magnetometer has a 1-sigma noise error of 10 nanoTesla. We also assume the 1-sigma ranging error to each MRR on the host target board is 1 cm.

Three-axis root-sum-squared relative navigation errors are provided in Figures 7 through 9 for a Kalman filter solution using a 10 Hz propagation rate and a 1 Hz measurement update rate. Unfiltered position errors with a 1-sigma error of about 1 cm, depicted in Figure 7, are consistent with the MRR ranging noise. Both unfiltered and filtered attitude errors, depicted in Figure 8, demonstrate the noise attenuation capability of the Kalman filter. In the upper plot the Earth sensor is utilized, resulting in a 1-sigma error of about 0.7 degrees for the unfiltered solution (the gray plot) and about 0.3 degrees for the filtered solution (the black plot). In the lower plot the magnetometer sensor is utilized, resulting in a 1-sigma error of about 1 degree for the unfiltered solution and about 0.4 degrees for the filtered solution. The twice-per-orbit error peaks and valleys in the lower plot are due to the time-varying angle between the laser vector and the geomagnetic field vector, ranging from 90 degrees to as low as 37 degrees. In contrast, for the upper plot the angle between the laser vector and the Earth nadir direction is consistently 90 degrees. The 1-sigma host rate errors of about 0.025 deg/sec using the Earth sensor and 0.033 deg/sec using the magnetometer, depicted in Figure 9, demonstrate the potential of the Kalman filter for estimating host inertial rates. It should be stated here that only a subset of the expected error terms listed in Table 1 were included in this simulation. Terms related to sensor biases, modeling errors, and laser gimbal angle errors were not included.

Preliminary Test Results

To demonstrate reflector discrimination capability, preliminary indoor laboratory tests were performed using a single MRR at a range of 39 meters.[17] To emulate two reflectors, two separate bit streams (one the mirror image of the other) were modulated from the single MRR, alternating at 10 second intervals. As shown in Figure 10, the pursuer transmitter/receiver system consisted of a two-axis gimbaled 100mW laser diode operating at a 976 nm wavelength, a silicon photodiode, signal amplifier, analog-to-digital converter, and two digital matched filters correlated to each bit stream sequence. The host MRR, shown in Figure 11, consisted of a 0.5 mm MQW retromodulator with a 30-degree field-of-view, and a three-point holder. The total MRR mass, including holder, was 10 grams and drew about 75 mW of power. A 15 volt swing was required to achieve sufficient on/off states. Reference 17 provides further details on the test setup.

Signal acquisition was achieved by performing a series of decreasing rectangular searches based on pre-defined threshold signal levels. As the laser beam crosses the MRR the return signal level increased and a threshold level was reached, initiating a smaller search pattern. This process was continued until the maximum signal level was obtained.

When a signal was received by the photodetector the receive algorithm processed the bit stream using the matched filters to determine which bit stream was being sent by the modulator (in effect, discriminating between the two streams). The outputs from the two matched filters are provided in Figure 12, where it is observed that the on/off modulation levels from each bit stream were properly matched and, hence, discriminated.

Future laboratory tests will utilize the target board in Figure 5, requiring five matched filters for each MRR. In those tests the MRR return signals will be sequenced at a rate of about 0.2 seconds, requiring about 1 second to process and discriminate between each reflector signal. That data will then be used to calculate the relative pose of the host platform, as described in this paper.

Conclusions

In this paper we described a novel concept for combined spacecraft-to-spacecraft laser interrogation, communication, and navigation utilizing a gimbaled laser source on the pursuer spacecraft and a target board

8

of modulating retroreflectors on the host spacecraft. Using time-of-flight range measurements to each retromodulator and the known laser gimbal angles, we discussed approaches for determining relative position and attitude of fully-cooperative, partially-cooperative, and non-cooperative hosts. Simulations demonstrated the potential of the concept for providing centimeter-level relative positioning and degree-level relative attitude for vehicle separation distances of tens of meters to kilometers. Preliminary experimental results demonstrated the capability of the pursuer detection electronics and software for discriminating between multiple modulated retroreflector signals.

References

1. Polites, M. E., "Technology of Automated Rendezvous and Capture in Space," **Journal of Spacecraft and Rockets**, Vol. 36. No. 2, March-April 1999, pp. 280-291.

2. Purcell, G., Kuang, D., Lichten, S., Wu, S. C., and Young, L., "Autonomous Formation Flyer (AFF) Sensor Technology Development," **21st Annual AAS Guidance and Control Conference**, Breckenridge, CO, Feb. 4-8, 1998.

3. Junkins, J. L., Hughes, D., Wazni, K., and Pariyapong, V., "Vision-Based Navigation for Rendezvous, Docking, and Proximity Operations," **22nd Annual AAS Guidance and Control Conference**, Breckenridge, CO, Feb. 3-7, 1999.

4. Mokuno, M., Kawano, I., and Kasai, T., "Experimental Results of Autonomous Rendezvous Docking on Japanese ETS-VII Satellite," **22nd Annual AAS Guidance and Control Conference**, Breckenridge, CO, Feb. 3-7, 1999.

5. D'Souza, C., Bognar, A., and Brand, T., "An Evaluation of the GPS Relative Navigation System for ETS-VII and HTV," **22nd Annual AAS Guidance and Control Conference**, Breckenridge, CO, Feb. 3-7, 1999.

6. Cislaghi, M., Fehse, W., Paris, D., and Ankerson, F., "The ATV Rendezvous Predevelopment Programme (ARP)," **22nd Annual AAS Guidance and Control Conference**, Breckenridge, CO, Feb. 3-7, 1999.

7. Howard, R. T., Bryan, T. C., Book, M. L., and Dabney, R. W., "The Video Guidance Sensor – A Flight Proven Technology," **22nd Annual AAS Guidance and Control Conference**, Breckenridge, CO, Feb. 3-7, 1999.

8. Cruzen, C. A., Lomas, J. J., and Dabney, R. W., "Test Results for the Automated Rendezvous and Capture System," **23nd Annual AAS Guidance and Control Conference**, Breckenridge, CO, Feb. 2-6, 2000.

9. Hollander, S., "Autonomous Space Robotics: Enabling Technologies for Advanced Space Platforms," **Space 2000 Conference and Exposition**, Long Beach, CA, Sept. 19-21, 2000.

10. Gilbreath, G. C., Bowman, S. R., Rabinovich, W. S., Merk, C. H., and Senasack, H. E., "Modulating Retroreflector Using Multiple Quantum Well Technology," **U. S. Patent No. 6,154,299**, awarded November, 2000.

11. Gilbreath, G. C., et al., "Compact, Lightweight Payload for Covert Data Link using a Multiple Quantum Well Modulating Retroreflector on a Small Rotary Wing Unmanned Airborne Vehicle," **SPIE Annual Meeting Proceedings**, 4127, pp. 57-67, 2000.

12. Katzer, D. S., Rabinovich, W. S., Ikossi-Anastasiou, K., and Gilbreath, G. C., "Optimization of Buffer Layers for InGaAs/AlGaAs PIN Optical Modulators Grown on GaAs Substrates by Molecular Beam Epitaxy," **Journal of Vacuum Science Technology**, B 18, pp. 1609-1613, 2000.

13. Kyono, C. S., et al., "GaAs/AlGaAs Multiquantum Well Resonant Photorefractive Devices Fabricated using Epitaxial Liftoff," **Applied Physics Letters**, 64 (17), pp. 2244-2246, April, 1994.

14. Goetz, P. G., et al., "Effects of Proton Irradiation on InGaAs/AlGaAs Multiple Quantum Well Modulators," **IEEE Aerosense Conference**, Paper No. 5.0402, March, 2001.

15. Shuster, M. D. and Oh, S. D., "Three-Axis Attitude Determination from Vector Observations," **Journal of Guidance and Control**, Vol. 4, No. 1, Jan-Feb, 1981, pp. 70-77.

16. Creamer, G., "Spacecraft Attitude Determination Using Gyros and Quaternion Measurements," **The Journal of the Astronautical Sciences**, Vol. 44, No. 3, July-Sept, 1996, pp. 357-371.

17. Gilbreath, G. C., et al., "Retromodulator for Optical Tagging for LEO Consumables," **IEEE Aerosense Conference**, Paper No. 5.0403, March, 2001.
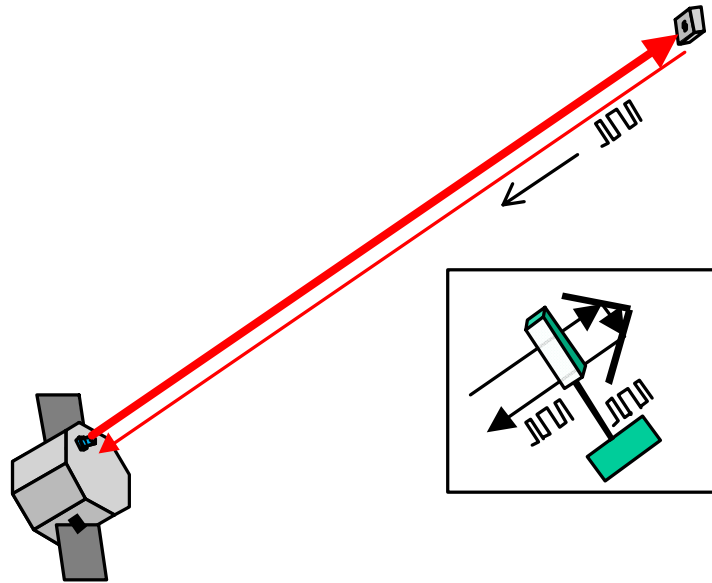
Glenn Creamer

Figure 1: Concept for MQW Retromodulators used as ID Tags
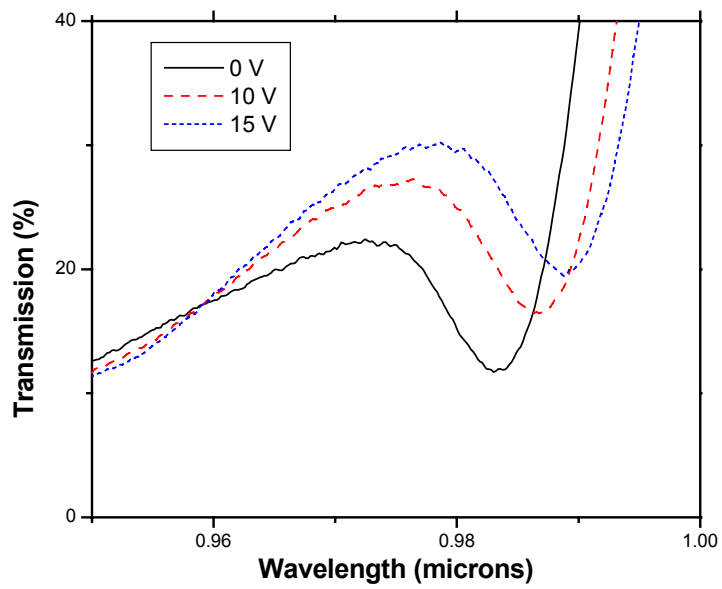

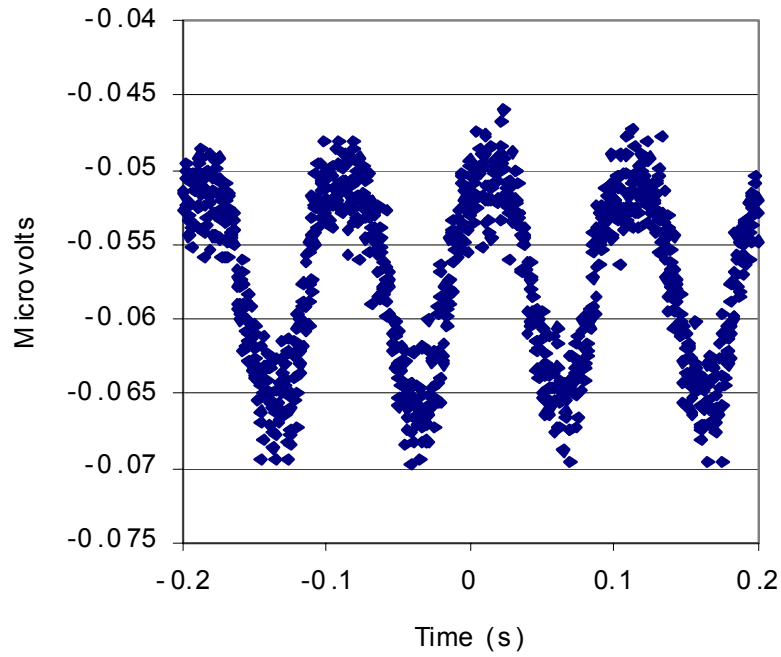**Figure 2: Transmission Performance for an InGaAs-Based MQW Modulator**
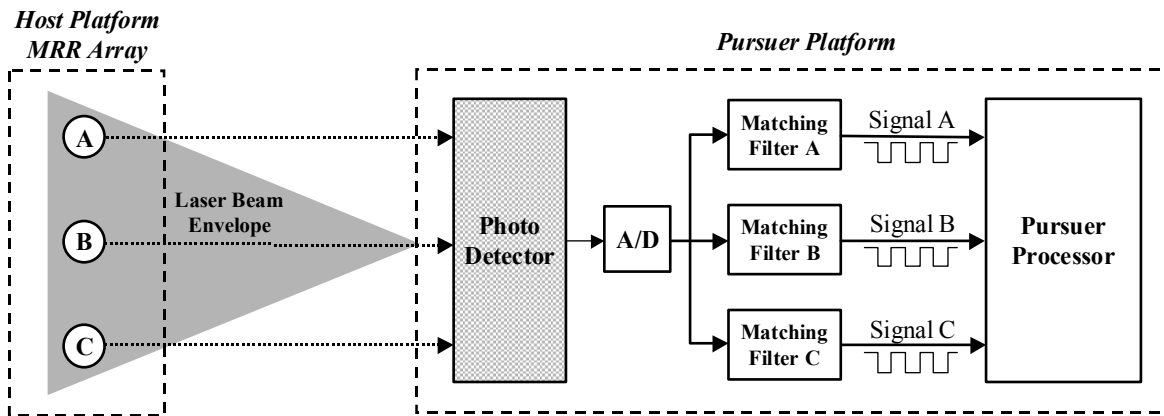
Figure 3: Waveform for a 9-Segmented Modulator

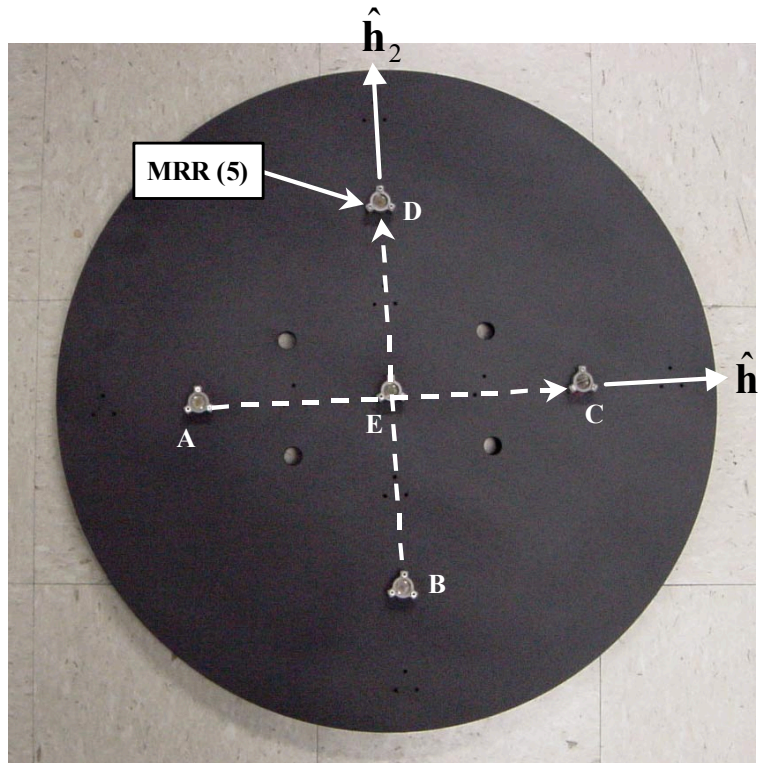**Figure 4: Platform-to-Platform Communication and MRR Discrimination Strategy**
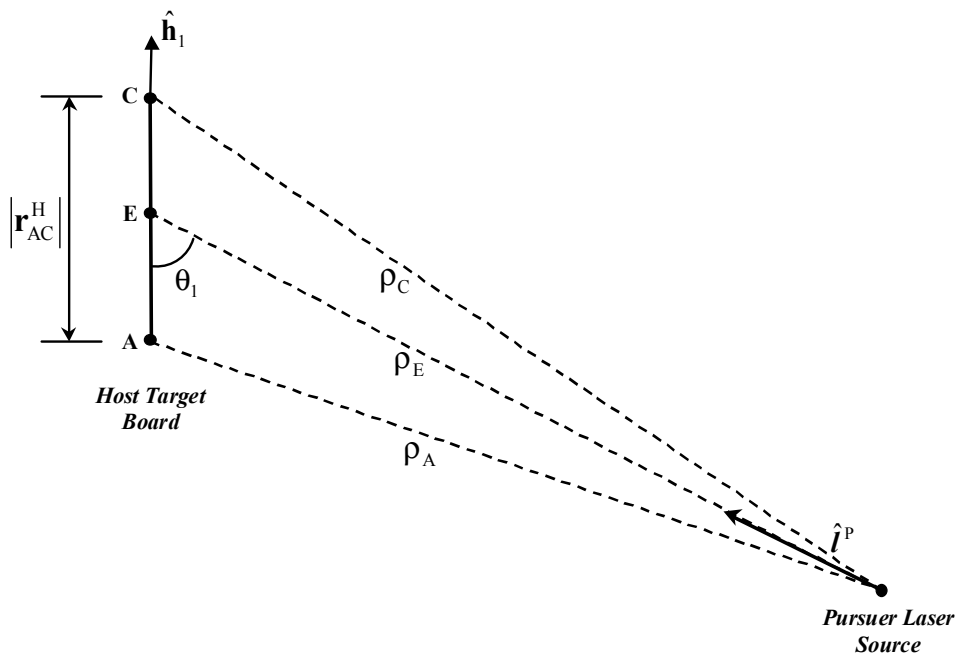
11

Figure 5: MRR Target Board Layout

Figure 6: Planar Ranging Geometry

Glenn Creamer   15th Annual AIAA/USU Conference on Small Satellites

Table 1: Potential System Errors

Error Source	Expected Value (3-sigma)
Sensor Errors	
Time-of-Flight	1 - 2 cm
Entity Vector Measurement	0.1 - 1 deg
Laser Gimbal Angles	5 - 10 arcsec
Modeling Errors	
Baseline Knowledge	1 - 2 mm
Entity Vector Orientation (Non-Cooperative Hosts)	1 - 10 deg
Geometric Errors	
Co-Linearity of Laser and Entity Vectors	Inversely Proportional to Included Angle
Range-Sensitive Laser Gimbal Angles	Baseline Length / (4*Range)
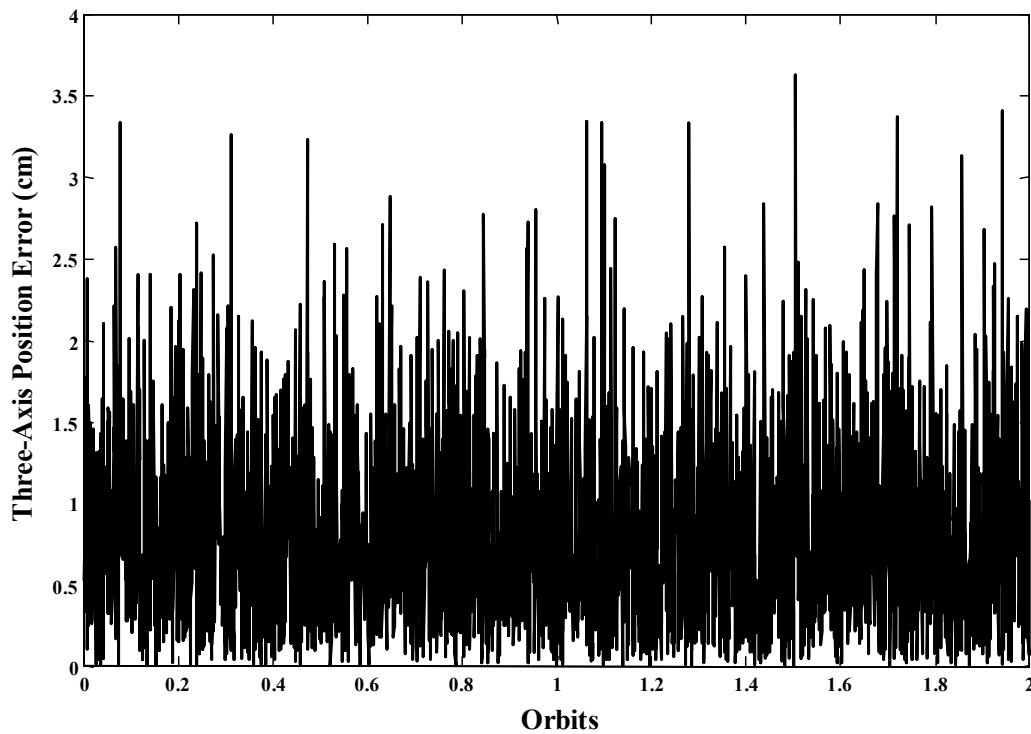
Figure 7: Simulated Three-Axis Root-Sum-Squared Position Errors
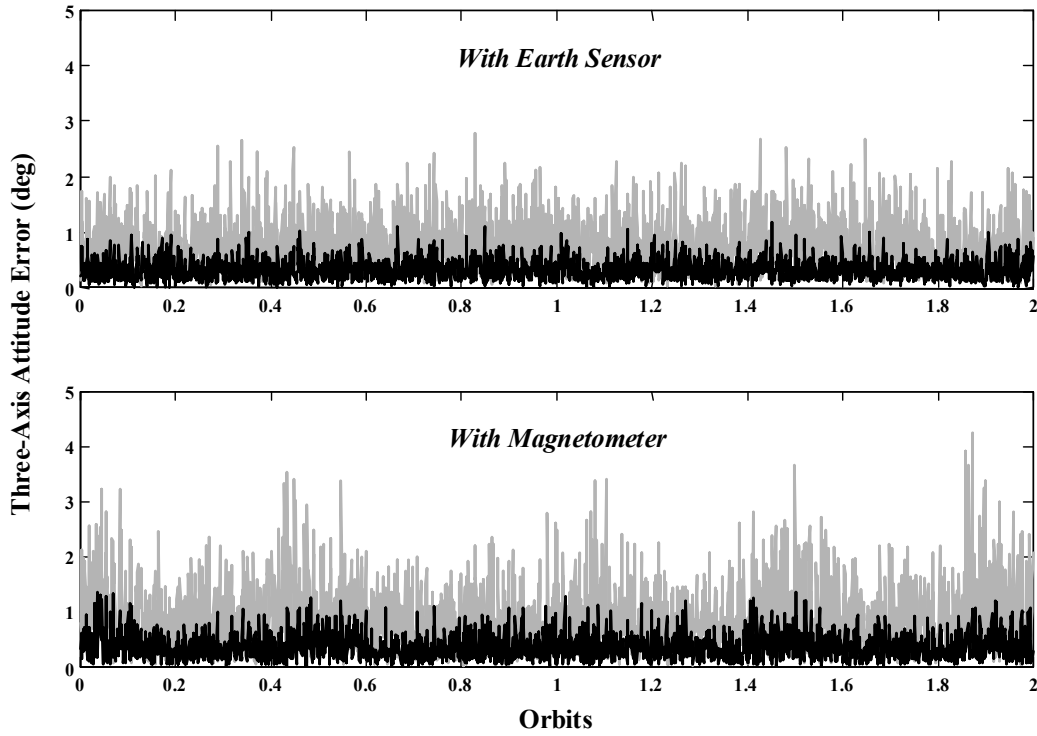
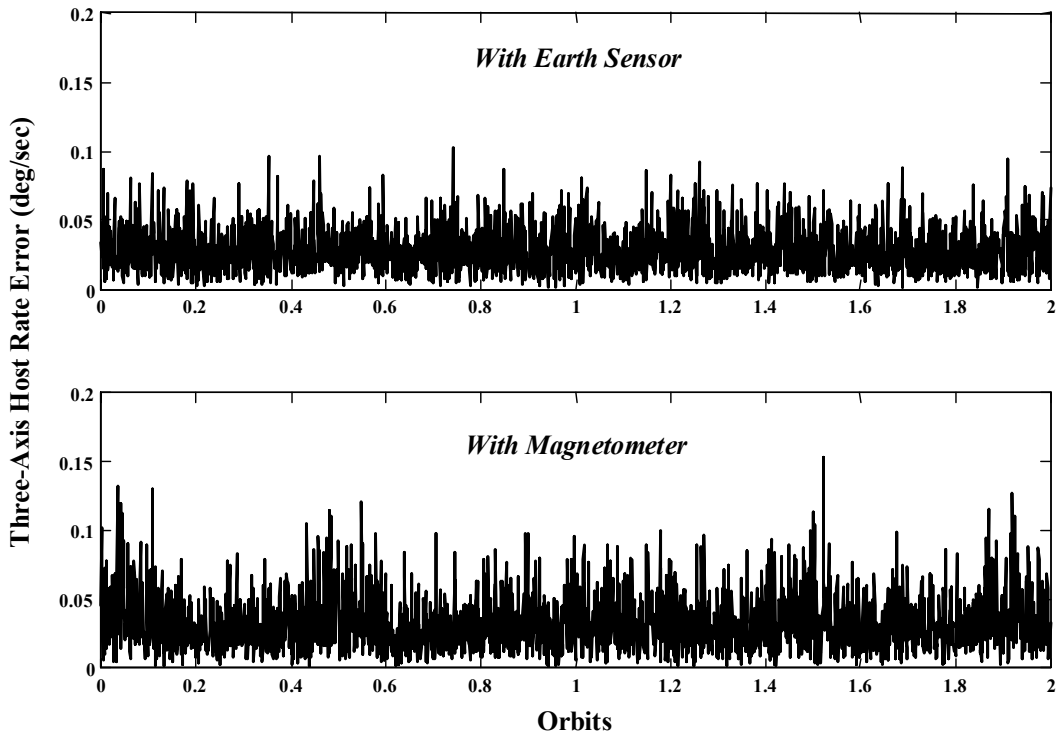**Figure 8: Simulated Three-Axis Root-Sum-Squared Attitude Errors**

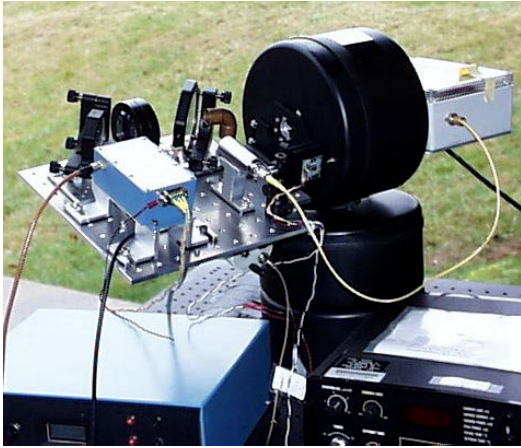**Figure 9: Simulated Three-Axis Root-Sum-Squared Host Rate Errors**
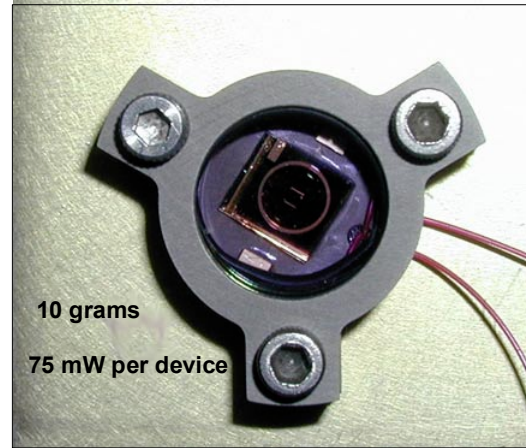
14

Figure 10: Optical Transmitter/Receiver System

10 grams

75 mW per device

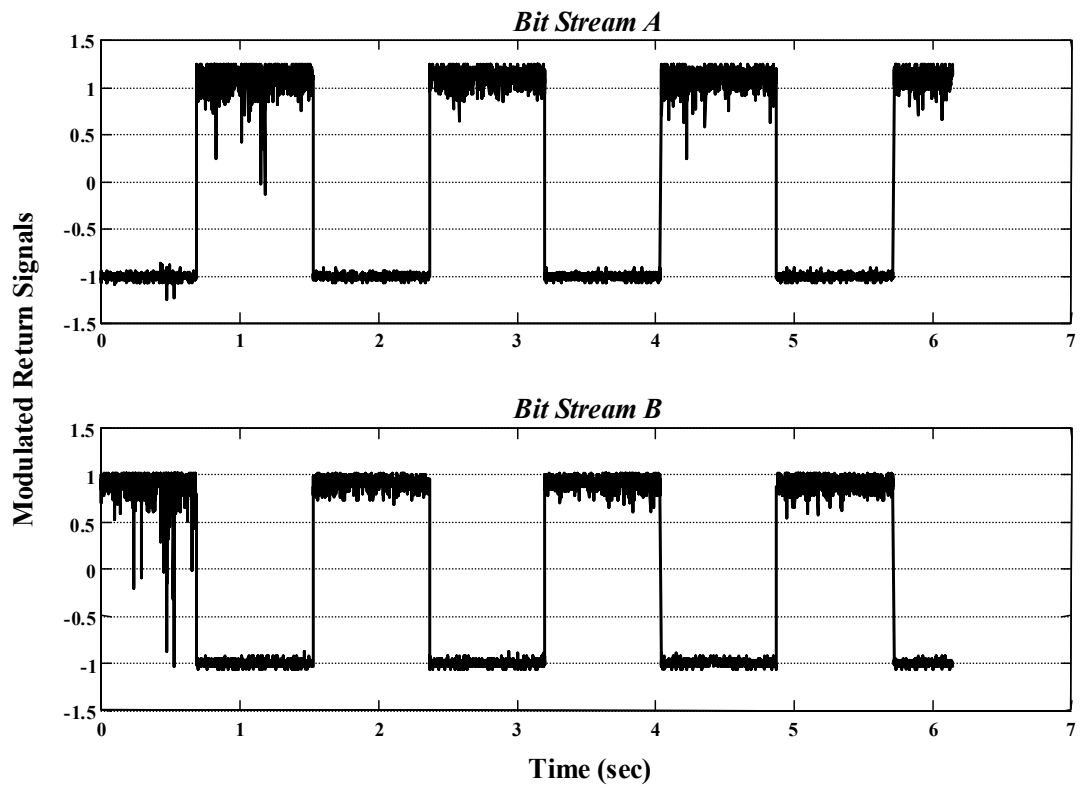**Figure 11: Mounted Modulating Retroreflector**

Figure 12: Experimental Results Demonstrating Dual Bit Stream Tracking

15

Dr. Glenn Creamer received his B. S. degree in Aerospace Engineering from Texas A&M University and his M. S. and Ph. D. degrees in Engineering Science and Mechanics from Virginia Tech. He has been with the Naval Center for Space Technology at NRL since 1989, specializing in spacecraft attitude determination and control.

Dr. Charmaine Gilbreath receiver her B. S. degree in Physics from Georgia Tech, her MSE and Ph. D. degrees in Electrical Engineering from The Johns Hopkins University. She has been at NRL since 1982, specializing in nonlinear optics, free space optical data transfer, and optical device development.

Mr. Timothy Meehan received his BSEE from the University of Maryland and his MSEE from the Johns Hopkins University. He has been with NRL since 1993, and serves as the electronics lead for the MQW modulating retroreflector program.

Ms. Mena Ferraro Stell received the B. S. degree in Aerospace Engineering and the B. S. degree in Applied Physics from the Illinois Institute of Technology. She works in the Electro-Optics Technology section of the Space Systems Development Department at NRL under contract with RSI, Inc.

Mr. Michael Vilcheck received his B. S. degree in Physics from Allegheny College, and is currently working toward an M. S. degree in Mechanical Engineering at the University of Maryland. He works as a physicist for the Electro-Optics Section of the Naval Center for Space Technology at NRL, with research interests in free space optical communication, satellite laser ranging, and atmospheric turbulence study.

Dr. William Rabinovich received the B. S. degree in Physics from the State University of New York at Stony Brook, and his M. S. and Ph. D. degrees in Physics from Brown University. He has been with NRL since 1987, and is currently Head of the Photonics Materials and Devices Section.